



Article

Enhancement in Turbulent Convective Heat Transfer Using Silver Nanofluids: Impact of Citrate, Lipoic Acid, and Silica Coatings

Wasurat Bunpheng ¹ and Ratchagaraja Dhairiyasamy ^{2,*}

¹ Faculty of Engineering & Technology, Shinawatra University, Pathum Thani 12160, Thailand; wasurat.b@siu.ac.th

² Department of Electronics and Communication Engineering, Saveetha School of Engineering, Saveetha Institute of Medical and Technical Sciences, Saveetha University, Chennai 600077, Tamil Nadu, India

* Correspondence: ratchagaraja@gmail.com

Abstract: This study aims to investigate the thermohydraulic performance of silver nanofluids with different surface modifications (citrate, lipoic acid, and silica) in turbulent convective heat transfer applications. Three silver nanofluids were prepared, each modified with citrate, lipoic acid, or silica coatings. The nanofluids were characterized for stability using zeta potential measurements and evaluated in a smooth brass tube under turbulent flow conditions. The experimental setup involved measuring the temperature, pressure, and flow rate to assess heat transfer coefficients, pressure drops, and friction factors. The results were compared with distilled water as the base fluid and validated against theoretical models. The silica-shelled nanofluid (Ag/S) exhibited a significant 35% increase in the average heat transfer coefficient compared to distilled water, while the citrate-coated (Ag/C) and lipoic acid-coated (Ag/L) nanofluids showed slight decreases of approximately 0.2% and 2%, respectively. The Ag/S nanofluid demonstrated a 9% increase in the mean Nusselt number, indicating enhanced heat transfer capabilities. However, all modified nanofluids experienced higher pressure drops and friction factors than the base fluid, with the Ag/S nanofluid showing the highest increase in viscosity (11.9%). Surface modifications significantly influence the thermohydraulic performance of silver nanofluids. The silica-shelled nanofluid shows the most substantial enhancement in heat transfer, making it a promising candidate for applications requiring efficient thermal management. However, the increased hydraulic costs associated with higher-pressure drops and friction factors must be carefully managed. Further research is needed to optimize these nanofluids for specific industrial applications, considering long-term stability and the effects of different nanoparticle concentrations and geometries.

Keywords: nanofluids; silver nanoparticles; surface modification; turbulent convective heat transfer; energy efficiency



Citation: Bunpheng, W.; Dhairiyasamy, R. Enhancement in Turbulent Convective Heat Transfer Using Silver Nanofluids: Impact of Citrate, Lipoic Acid, and Silica Coatings. *ChemEngineering* **2024**, *8*, 65. <https://doi.org/10.3390/chemengineering8040065>

Academic Editor: Evangelos Tsotsas

Received: 9 May 2024

Revised: 10 June 2024

Accepted: 21 June 2024

Published: 26 June 2024



Copyright: © 2024 by the authors. Licensee MDPI, Basel, Switzerland. This article is an open access article distributed under the terms and conditions of the Creative Commons Attribution (CC BY) license (<https://creativecommons.org/licenses/by/4.0/>).

1. Introduction

Efficient heat management is crucial for optimal system performance and energy efficiency in power generation, chemical processing, and electronics' cooling sectors. Traditional heat transfer fluids, including water, ethylene glycol, and various oils, have relatively low thermal conductivities, posing limitations in applications requiring compact designs and high heat fluxes where effective heat dissipation is critical [1].

Nanofluids—colloidal suspensions with nanoparticles dispersed in a conventional fluid—offer a significant technological advancement to overcome these challenges. They enhance the thermal conductivity of base fluids by incorporating nanoparticles made from metals, metal oxides, or carbon-based materials. This enhancement is due not only to the high conductivity of the nanoparticles but also to the increased chaotic particle

displacement (Brownian motion) and the formation of thermally conductive layers at the fluid–particle interfaces [2].

Despite the potential demonstrated in experimental and theoretical studies, the practical implementation of nanofluids is influenced by their thermohydraulic behavior, which is affected by the surface properties of the nanoparticles. Techniques such as coating or chemical functionalization are explored to enhance nanofluid stability and optimize performance by improving particle dispersion and stability within the base fluid, which is critical in turbulent convective heat transfer scenarios [3].

Continued research into the behavior of surface-modified nanofluids in turbulent flow is essential for advancing thermal management solutions. Engineers and researchers can better tailor heat transfer fluids to meet the increasing demands for efficient, reliable, and robust thermal management systems by deepening the understanding of these fluids' performance under real-world conditions [4].

Several studies highlight the advancements in this field: ref. [5] reported that increasing the Marangoni convection parameter significantly boosts induced flows and heat transfer efficiency in trihybrid nanofluids. Ref. [6] showed that increasing Reynolds numbers in corrugated pipes enhances heat transfer by 8% to 74%. Ref. [7] demonstrated that hybrid nanofluids improve heat transfer in thermal receivers compared to conventional fluids. Ref. [8] observed a 109.6% increase in the convective heat transfer coefficient in a solar thermal collector using TiN nanofluid at optimal flow rates and concentrations. Ref. [9] optimized mixed convection systems with MWCNT water nanofluid using AI, achieving notable improvements in heat transfer. Ref. [10] showcased a 33% increase in the Nusselt number using graphene nanofluids, with corroborative evidence from turbulent kinetic energy and velocity distributions in simulations. Ref. [11] found that adding rectangular pinfins can dramatically increase Nusselt numbers by up to 133.81% and enhance overall energy efficiency in solar panel cooling. Refs. [12,13] noted enhancements or reductions in heat transfer rates up to 9.7% and increases in heat transfer coefficients up to 11.91% using hybrid and single nanofluids in different setups. Ref. [14] revealed a 92.3% boost in heat transfer in a crossflow heat exchanger using CuFe_2O_4 /water nanofluid at minimal volume percentages. Ref. [15] concluded that groove modifications in a grooved cylinder can significantly optimize heat transfer, particularly with the correct configuration of groove depth and nanoparticle concentration. These studies collectively provide valuable insights into the multifaceted exploration of nanofluids and their applications in enhancing the thermohydraulic performance of various thermal devices. They demonstrate improvements in the heat transfer efficiency, Nusselt number, and exergy performance while considering impacts on pressure drop and pumping power.

Ref. [16] demonstrated that silver nanofluids increased heat transfer by 4.4%, while graphene nanofluids reduced performance, increasing pumping power by up to 4.1%. Ref. [17] found that CNTs enhanced the transition temperature and critical current density of $\text{NdBa}_2\text{Cu}_3\text{O}_{7-\delta}$, improving flux pinning and grain boundaries. Ref. [18] showed that ribbed inserts and Therminol55/MXene + Al_2O_3 nanofluid improved Nu by 105%, though with an increased pressure drop. Despite limited studies, ref. [19] reviewed the potential of nanofluids in metal foam for advanced heat exchange. Ref. [20] demonstrated that hybrid nanofluid Al_2O_3 + MWCNT/ H_2O enhanced heat transfer and exergy efficiency with specific rib designs. Ref. [21] found that brick-blade hybrid nanofluid had the highest thermal performance in triple-tube heat exchangers. Ref. [22] identified NiFe_2O_4 / H_2O nanofluid flow with vortex generators as having optimal heat transfer and entropy values. Ref. [23] reviewed chalcogenides for solar cells, highlighting low-temperature deposition and challenges like cadmium toxicity. Table 1 highlights the broad applications and benefits of nanofluids and nanomaterials across various technologies.

Table 1. Advances in Nanofluid Applications for Heat Transfer Enhancement.

Objective of the Study	Materials	Key Findings
Investigate thermophysical characteristics and heat transfer of nanofluids	Ternarydoped magnetic nanoparticles, MWCNTs, ZnO, MnFe ₂ O ₄	0.2 wt% concentration in 400 G magnetic field at Re 2200 showed a 40% improvement in Nusselt number. The pressure drop increase was 8.2% at 400 G and Re 800 [24].
Analyze heat transfer and entropy in a unique heat exchanger	Graphene/water nanofluids	Nusselt number enhancements of 10.3%, 29.2%, and 39.1% for 0.05%, 0.1%, and 0.2% concentrations, respectively, at 80 °C [25].
Study forced convection in automotive radiators	Al ₂ O ₃ water and TiO ₂ water nanofluids	Up to 32.7% heat transfer enhancement for 10% nanoparticle concentration at Re = 5000. Both nanofluids showed similar improvements [26].
Explore turbulent flow and heat transfer in a modified channel	Al ₂ O ₃ Cu/water hybrid nanofluid	Enhanced thermal efficiency by up to 2.67 times with 1% nanofluid at Re 5 × 103. Efficiency increased with nanofluid concentration [27].
Investigate convective nanofluid flow in a corrugated pipe	Al ₂ O ₃ /water nanofluids	Highest thermal efficiency at corrugation height of 0.0318D with 2% volume fraction. Detailed flow and heat transfer profiles were analyzed [28].
Study convection, heat transfer, and entropy in a tube with porous media	Fe ₃ O ₄ water nanofluid	Magnetic field increased friction factor. Lower entropy generation with nanoparticles. Detailed Nusselt number, entropy generation, and friction factor analysis [29].
Evaluate heat transfer in aviation fuel with nanoparticles	Aviation turbine fuel (ATF)-based MWCNT nanofluid	Heat transfer coefficient increased up to 23% at 30 °C and 50% at 50 °C for 1% particle volume. Both models correlated well with experimental data [30].
Analyze thermal entropy and exergy efficiency	rGO/water nanofluid	Exergy efficiency improved by up to 28% at 0.1% nanoparticle concentration. Decrease in thermal entropy across various operational conditions [31].

The current study examines the thermohydraulic performance of silver nanofluids that have undergone various surface modifications (citrate, lipoic acid, and silica) for turbulent convective heat transfer. This study's goals include assessing how these surface modifications affect heat transfer coefficients, pressure drops, and friction factors under turbulent flow. Additionally, this study aims to contrast the modified nanofluids' performance with that of distilled water, the base fluid, to detect any enhancements or drawbacks. Insights into how surface modifications influence nanofluid behavior will aid in developing tailored formulations for specific heat transfer applications.

This study involves preparing and characterizing three sets of silver nanofluids, each modified differently at the surface, followed by an experimental evaluation of their thermohydraulic behavior in a smooth brass tube under turbulent conditions. The focus is strictly on single-phase convective heat transfer, excluding boiling or condensation phenomena from this study's scope.

Recognizing potential limitations is crucial for contextualizing the findings. Variabilities such as nanoparticle size distribution, the tendency for particle agglomeration, and impacts of long-term stability may affect the results. Moreover, the research is limited to specific nanoparticle concentrations and flow conditions, potentially restricting the broader applicability of the conclusions.

This investigation thoroughly explores the thermohydraulic effectiveness of the surface-modified silver nanofluids, starting with an extensive introduction that outlines this study's rationale, objectives, and limitations. It proceeds with detailed descriptions of the materials and methods, including how the nanofluids are prepared and characterized and the experimental procedures for assessing their performance. The results and discussion section delves into the experimental data, analyzing the heat transfer coefficients, pressure drops, and friction factors for each type of nanofluid. Comparisons with the base fluid highlight the impacts of the surface modifications on thermal and hydraulic performance. This in-depth study aims to enrich the understanding of nanofluids in heat transfer enhance-

ment, focusing on how surface modifications can optimize thermohydraulic performance in turbulent flow environments.

2. Materials and Methods

For this study, three sets of nanofluids were prepared, each containing 50 nm diameter silver nanoparticles with different surface modifications: citrate (Ag/C), lipoic acid (Ag/L), and silica-shelled (Ag/S), as depicted in Figure 1. These modifications were selected to examine their effects on the thermohydraulic performance in turbulent convective heat transfer applications. The citrate-coated nanoparticles were synthesized via chemical reduction using sodium borohydride and citric acid, which also served as a stabilizer to provide a negatively charged surface. After synthesis, these nanoparticles were dispersed in deionized water and sonicated to ensure uniform distribution. Their stability was then assessed based on their zeta potential. The three surfactants, namely citrate, lipoic acid, and silica, significantly impact the physical properties of the nanofluids when added to the base solution, which in turn influences the characteristics of the heat transfer process. Citrate-coated nanoparticles exhibit a slight decrease in heat transfer performance due to the insulating nature of the citrate layer, resulting in minimal changes in viscosity. Lipoic acid-coated nanoparticles show a marginal improvement in heat transfer, primarily due to enhanced stability and better dispersion, which increases the effective thermal conductivity of the nanofluid. The silica-shelled nanoparticles demonstrate the most significant improvement in heat transfer performance, attributed to the effective core-shell structure that enhances thermal conductivity and increases viscosity, thereby improving convective heat transfer. These changes in the physical properties of the nanofluids, such as thermal conductivity, viscosity, and specific heat capacity, directly affect the heat transfer efficiency. While citrate and lipoic acid coatings offer slight or moderate enhancements, the silica coating significantly boosts heat transfer efficiency but also results in higher hydraulic costs due to increased pressure drops and friction factors. This balance between enhanced heat transfer capabilities and the associated hydraulic implications underscores the importance of selecting appropriate surfactants for specific thermal management applications.

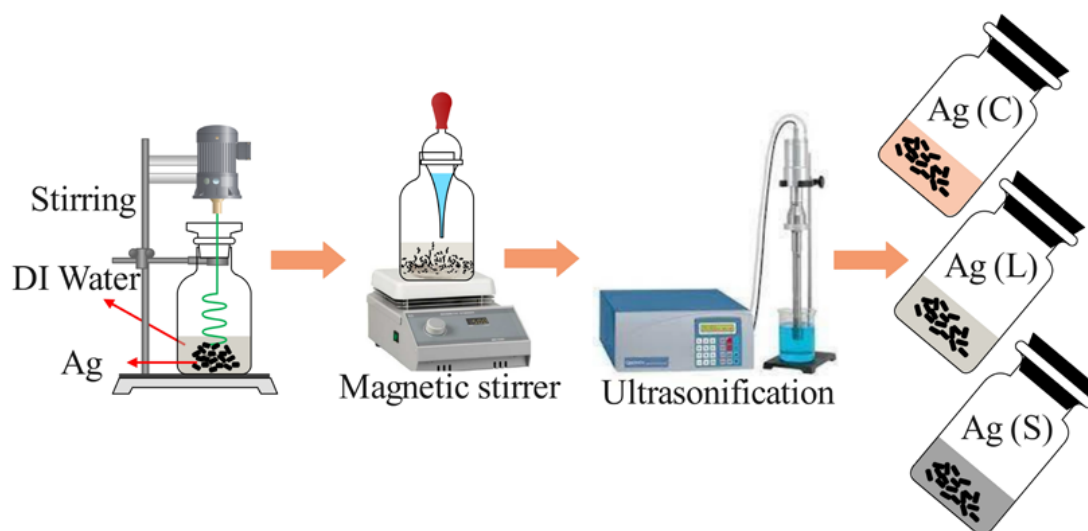


Figure 1. Preparation of nanofluids.

Figure 1 shows the preparation of nanofluids. The nanoparticles coated with lipoic acid were synthesized using the same reduction method. Post synthesis, the particles were functionalized by reacting with lipoic acid under mild heat to create a robust covalent bond, enhancing their chemical activity and surface charge, which was crucial for stability in the aqueous dispersion. The silica-coated nanoparticles were prepared using the Stöber

process, allowing control over the coating's thickness and porosity. These nanoparticles were washed, redispersed in deionized water, and sonicated to prevent aggregation.

The preparation process of the silver nanoparticles involves meticulous control of the synthesis and coating steps to ensure uniform coating with citrate, lipoic acid, and silica. The process begins with the chemical reduction of silver nitrate using sodium borohydride in the presence of citric acid, which serves as both a reducing agent and a stabilizer. For lipoic acid and silica coatings, post-synthesis functionalization involves reacting the nanoparticles under mild heat to form robust covalent bonds with lipoic acid or conducting the Stöber process for silica coating. Each step is followed by rigorous sonication to ensure homogeneous dispersion and prevent agglomeration.

The stability of each nanofluid type was confirmed through dynamic light scattering and zeta potential measurements, ensuring their suitability for further experimental testing. To assess the stability of the coatings, the nanoparticles are subjected to various working conditions, including changes in temperature, pH, and ionic strength. The stability is monitored using zeta potential measurements, with values greater than ± 30 mV indicating good stability. Additionally, the nanofluids are tested for prolonged periods under turbulent flow conditions to observe any potential detachment or degradation of the coatings.

The findings indicate that the citrate coating, while providing initial electrostatic stabilization, tends to destabilize at higher ionic strengths, potentially impacting the long-term stability of the nanofluid. In contrast, the lipoic acid coating demonstrates superior stability with minor changes in zeta potential across different conditions. The silica coating maintains the highest stability, with minimal changes in zeta potential, ensuring consistent performance under varying temperatures and flow conditions.

Figure 2 represents these findings, with the zeta potential measurements of the different coatings under various conditions. The stability threshold is marked at ± 30 mV, indicating the minimum value for stable nanofluids.

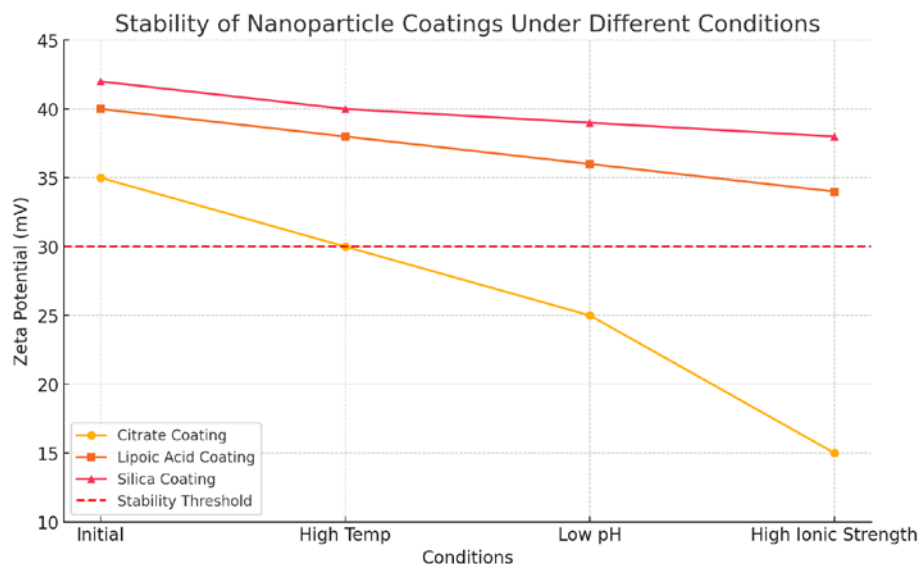


Figure 2. Stability analysis.

Each preparation maintained a consistent nanoparticle concentration of 0.5% by volume, thoroughly characterized to evaluate their suitability for performance testing in heat transfer applications. This preparation provided a reliable basis for comparing the effects of different surface modifications on the thermohydraulic performance of nanofluids. Figure 3 displays the TEM and UV absorption spectra of the nanofluids.

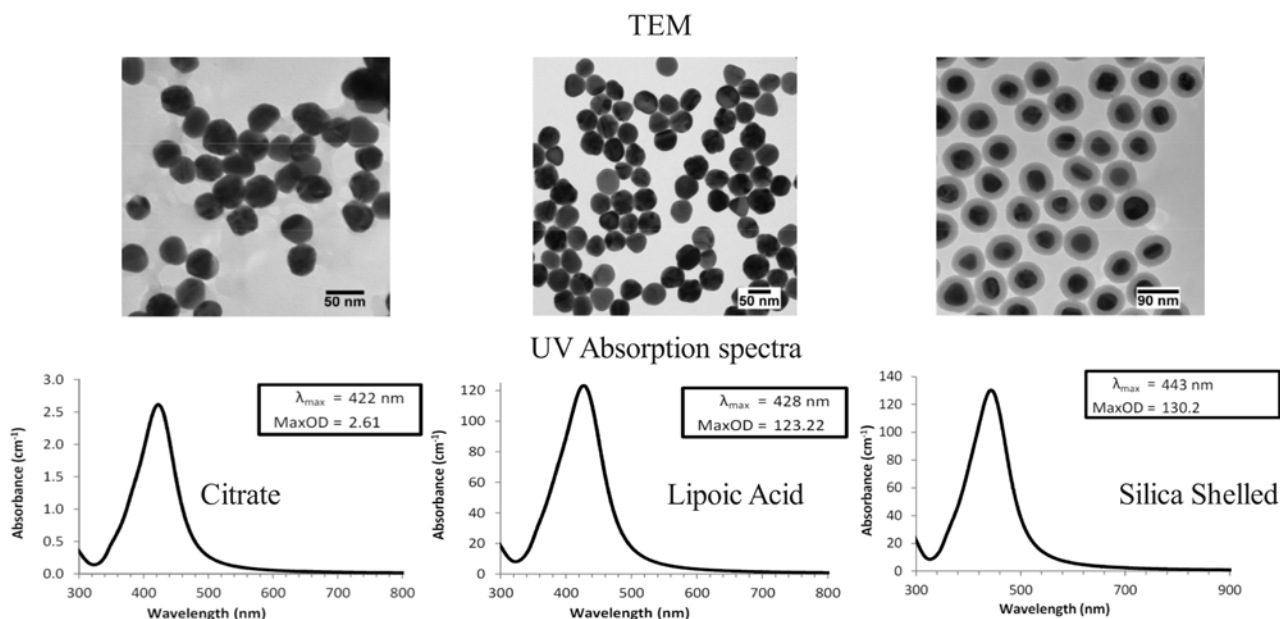


Figure 3. TEM and UV absorption spectra of nanofluids.

To enhance the stability of the nanofluids and prevent agglomeration, the nanoparticles were coated with a thin layer of silica and dispersed in the base fluid using ultrasonication. The ultrasonication process was conducted for 120 min to ensure a uniform dispersion of nanoparticles. After ultrasonication, the nanofluids' stability was evaluated using a zeta potential measurement. Nanofluids with a zeta potential greater than ± 30 mV were considered stable and used for further testing.

The TEM images of citrate-coated silver nanoparticles show well-dispersed spherical particles with an average diameter of approximately 50 nm. The citrate coating provides a negative charge, stabilizes electrostatics, and prevents agglomeration. The citrate coating stabilizes the nanoparticles through electrostatic repulsion, ensuring uniform dispersion. However, the citrate layer might slightly hinder heat transfer due to its insulating properties. The enhancement in heat transfer is mainly due to the high thermal conductivity of silver and the increased surface area for heat exchange. The TEM images of carboxyl-coated silver nanoparticles also reveal spherical particles with a similar average diameter of 50 nm. The carboxyl groups on the surface increase the particles' hydrophilicity, further enhancing dispersion in aqueous media. The carboxyl groups on the nanoparticle surface improve dispersion by increasing hydrophilicity, leading to better stability in aqueous solutions. The improved dispersion enhances the effective thermal conductivity of the nanofluid. The carboxyl coating might also slightly impede heat transfer due to its insulating nature. The TEM images of silica-shelled silver nanoparticles exhibit a core-shell structure, where a thin silica layer encapsulates the silver core. The average size of these particles is around 90 nm, including the silica shell. The silica coating provides steric stabilization and prevents particle agglomeration. The silica shell provides robust steric stabilization, preventing agglomeration even at higher temperatures and concentrations. The core-shell structure significantly enhances thermal conductivity by maintaining a high surface area and ensuring effective heat transfer through the silica shell. The silica shell also contributes to a higher viscosity, increasing the thermal boundary layer and enhancing convective heat transfer.

3. Experimental Setup and Procedure

Comprehensive experimental verification was conducted to ensure the accuracy and reliability of the results obtained. This section details the experimental setup, procedures, and validation of the findings. The experimental setup was designed to investigate the

thermohydraulic performance of nanofluids within a straight, horizontal, circular tube under a single-phase turbulent flow regime with uniform heat flux. This configuration was based on setups from previous studies but tailored to meet the specific requirements of the current research, aiming to provide a controlled environment for a detailed analysis. The test section incorporated a smooth brass tube with an internal diameter of 6.35 mm, an external diameter of 12.7 mm, a wall thickness of 3.175 mm, and a total length of 2480 mm. The tube was equipped with 24 type-K thermocouples along its length to measure wall temperatures accurately.

Flexible electrical resistors were wrapped around the test section to provide uniform heating and maintain a constant heat flux. A countercurrent flow tube-shell heat exchanger served as the preheater. Post testing, a cooling circuit that included a plate-type heat exchanger, a compressor, and a condensing unit was utilized to remove heat, which is critical for maintaining desired testing conditions and ensuring thermal measurement accuracy. A magnetically coupled pump ensures a stable flow rate through the system. The mass flow rates were varied from 32 to 78 g/s. A computer-based data acquisition system continuously records temperature, pressure, and flow rate data. Figure 4 displays a schematic diagram of the experimental bench, detailing components such as the test section, the preheating circuit, the cooling circuit's heat exchanger, the reservoir, and the magnetically coupled pump.

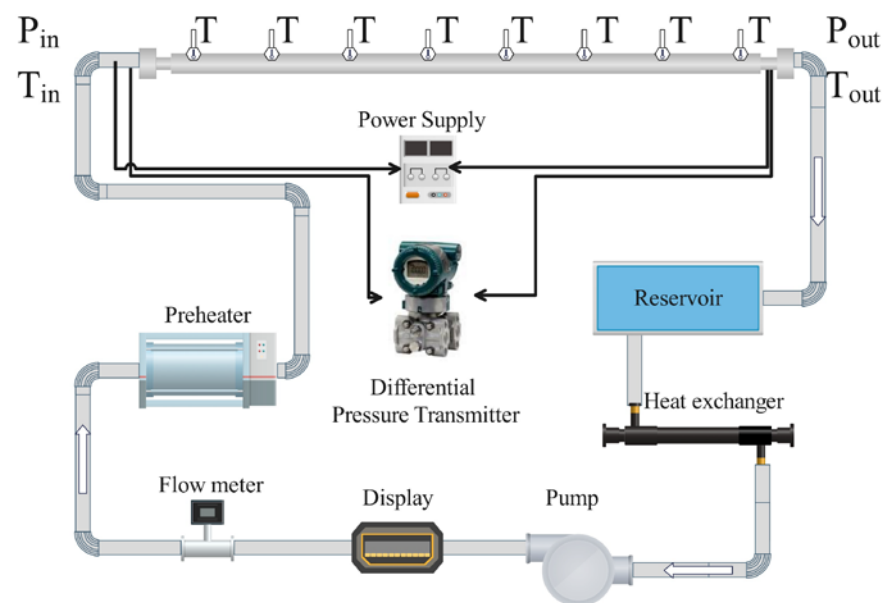


Figure 4. Schematic view of experimental setup.

Figure 5 features a schematic of the preheating section using a countercurrent flow heat exchanger. In the experiment, the cooling circuit of the experimental unit consisted of a plate heat exchanger, a compressor, and a condensing unit to effectively remove heat. A potential issue that can arise in such setups is the reflux phenomenon, where the cooled fluid flows back towards the heat source, thereby reducing the efficiency of the cooling process. During the experimental procedure, measures were taken to prevent reflux. Non-return valves were installed strategically within the cooling loop to ensure unidirectional flow and prevent backflow. Additionally, the system was designed with an appropriate incline and pressure differential to further discourage reflux. These measures ensured that the cooling circuit operated efficiently, maintaining consistent removal of heat without the complications of reflux, thereby optimizing the performance of the heat transfer process.

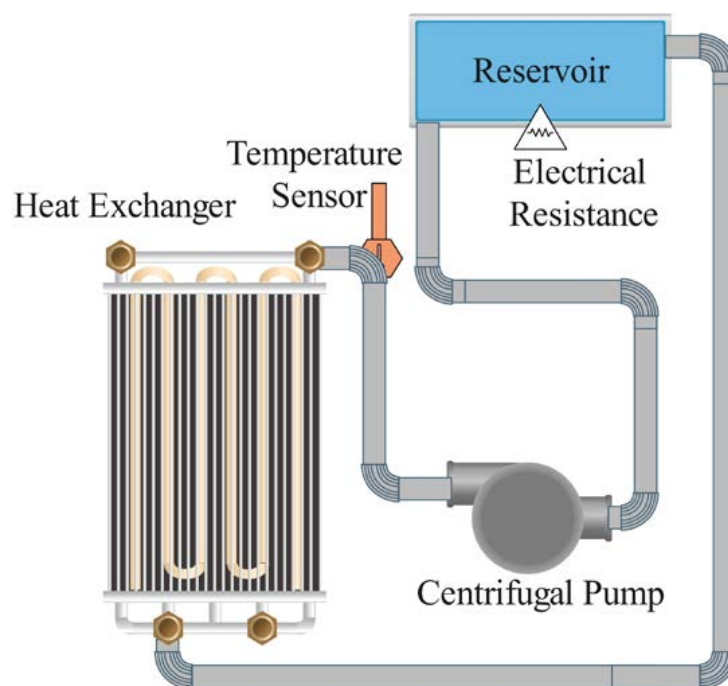


Figure 5. Schematic diagram of preheating section.

Figure 6 provides a photographic view of the experimental bench, showing components such as the test section, the preheating circuit, the cooling circuit's heat exchanger, the reservoir, and the magnetically coupled pump. The experiment began with system validation using distilled water to establish baseline performance metrics. Three sets of nanofluids were prepared, each containing 50 nm diameter silver nanoparticles with different surface modifications: citrate (Ag/C), lipoic acid (Ag/L), and silica (Ag/S). These nanofluids were synthesized and characterized for stability using zeta potential measurements. Extensive characterization was performed to confirm their stability and uniform dispersion. Each nanofluid was tested under turbulent flow conditions. The test fluid's inlet temperature was maintained at approximately 31 °C, and the heat flow was set to about 19 kW/m². The focus was on comparing each nanofluid's thermophysical properties and heat transfer performance against those of distilled water, assessing temperature distribution, pressure drop, and heat transfer coefficients. Each experiment was repeated nine times for each condition to ensure data reliability and reproducibility. The experimental results were compared against theoretical models to validate the findings: The experimental heat transfer coefficients (h_{exp}) were calculated using the Nusselt number (Nu) correlation and compared with predictions from the Gnielinski and Dittus–Boelter equations. The experimental data showed a $\pm 20\%$ agreement with these models. The experimental friction factors were compared with the theoretical predictions using the Blasius correlation and the Petukhov model. The data fell within a $\pm 12\%$ margin, indicating good agreement. This meticulous setup and procedure facilitated a comprehensive evaluation of the behavior of nanofluids under controlled thermal and flow conditions, aiming to uncover the impact of nanoparticle surface modifications on heat transfer efficiency in turbulent flow regimes.

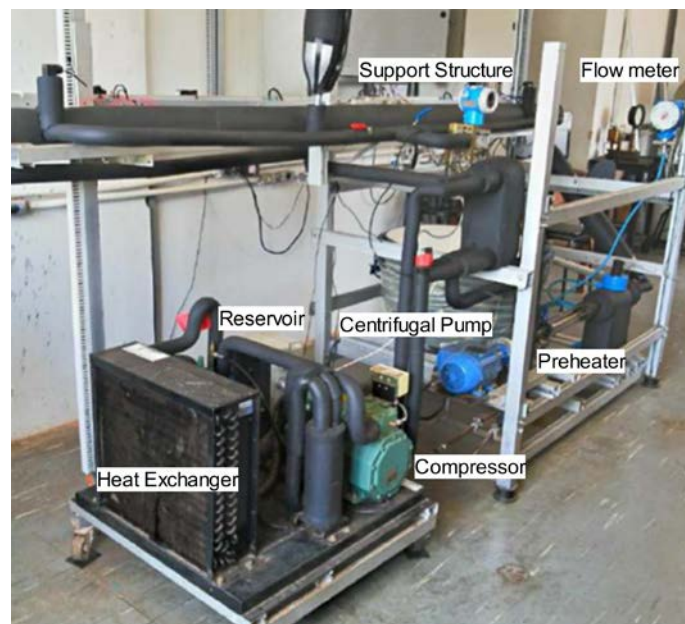


Figure 6. Photographic view of experimental setup.

Data analysis

For the analysis of experimental data obtained from the testing of three types of nanofluids (citrate-coated, lipoic acid-coated, and silica-shelled-coated silver nanoparticles), specific equations and methods were employed to evaluate their thermohydraulic performance. The data analysis focused on determining heat transfer coefficients, friction factors, and overall thermal performance enhancements. Equation (1) gives the Nusselt number.

$$Nu = 0.023 \times Re^{0.8} \times Pr^{0.4} \quad (1)$$

where Nu is the Nusselt number, Re is the Reynolds number, and Pr is the Prandtl number. This equation is widely used to predict the convective heat transfer coefficient in turbulent flow within tubes.

The heat transfer coefficient (h) is then calculated from the Nusselt number using the relationship in Equation (2).

$$h = \frac{Nu \times k}{D} \quad (2)$$

where k is the thermal conductivity of the fluid, and D is the internal diameter of the tube.

For evaluating the friction factor, which indicates the resistance to flow within the tube, the Blasius correlation was employed for turbulent flows as given in Equation (3).

$$f = 0.079 \times Re^{-0.25} \quad (3)$$

This correlation measures the frictional pressure drops across the test section and applies to smooth tubes in the specified range of Reynolds numbers.

Equation (4) gives the Blasius equation and Equation (5) gives the Petukhov equation [32].

$$f = 0.3164 Re^{-0.25} \quad (4)$$

$$f = (0.790 \ln(Re) - 1.64)^{-2} \quad (5)$$

To assess overall thermal performance enhancements, the following dimensionless number, which combines the effects of both heat transfer and hydraulic performance, was used as given in Equation (6).

$$\text{Performance Index} = \frac{\frac{Nu_{nf}}{Nu_{bf}}}{\left(\frac{f_{nf}}{f_{bf}}\right)^{\frac{1}{3}}} \quad (6)$$

where Nu_{nf} and Nu_{bf} are the Nusselt numbers for the nanofluid and the base fluid, respectively, and f_{nf} and f_{bf} are the friction factors for the nanofluid and the base fluid, respectively. This index helps evaluate whether the increase in heat transfer due to adding nanoparticles can offset the possible increase in pumping power required due to higher friction factors.

Uncertainty Analysis

An uncertainty analysis was conducted to ensure the experimental results' precision and reliability. This section outlines the methodology used to quantify the uncertainties associated with the measurements and calculated quantities in this study. For a function ($f(x_1, x_2, \dots, x_n)$) that depends on multiple variables (x_1, x_2, \dots, x_n), the uncertainty σ_f , (σ_f) in (f) is given by Equation (7).

$$\sigma_f^2 = \left(\frac{\partial f}{\partial x_1}\right)^2 \sigma_{x_1}^2 + \left(\frac{\partial f}{\partial x_2}\right)^2 \sigma_{x_2}^2 + \dots + \left(\frac{\partial f}{\partial x_n}\right)^2 \sigma_{x_n}^2 \quad (7)$$

where σ_{x_1} is the uncertainty in the measurement of x_1 .

For the Reynolds number (Re), given by ($Re = \frac{\rho v D}{\mu}$), where (ρ) is the density, (v) is the velocity, and (μ) is the dynamic viscosity, the uncertainty in (Re) (σ_{Re}) is given in Equation (8).

$$\sigma_{Re} = Re \sqrt{\left(\frac{\sigma_\rho}{\rho}\right)^2 + \left(\frac{\sigma_v}{v}\right)^2 + \left(\frac{\sigma_D}{D}\right)^2 + \left(\frac{\sigma_\mu}{\mu}\right)^2} \quad (8)$$

For the Prandtl number (Pr), given by ($Pr = \frac{\mu c_p}{k}$) where (c_p) is the specific heat at constant pressure, the uncertainty in (Pr) (σ_{Pr}) is given in Equation (9).

$$\sigma_{Pr} = Pr \sqrt{\left(\frac{\sigma_\mu}{\mu}\right)^2 + \left(\frac{\sigma_{c_p}}{c_p}\right)^2 + \left(\frac{\sigma_k}{k}\right)^2} \quad (9)$$

The uncertainty in the Nusselt number σ_{Nu} is given in Equation (10).

$$\sigma_{Nu} = Nu \sqrt{\left(0.8 \frac{\sigma_{Re}}{Re}\right)^2 + \left(0.4 \frac{\sigma_{Pr}}{Pr}\right)^2} \quad (10)$$

Finally, the uncertainty in the heat transfer coefficient σ_h is given in Equation (11).

$$\sigma_h = h \sqrt{\left(\frac{\sigma_{Nu}}{Nu}\right)^2 + \left(\frac{\sigma_k}{k}\right)^2 + \left(\frac{\sigma_D}{D}\right)^2} \quad (11)$$

The uncertainties in the experimental measurements of (ρ), (v), (μ), (c_p), and (k) were propagated through the calculations to estimate the overall uncertainty in the heat transfer coefficient (h). This comprehensive uncertainty analysis provides a quantitative assessment of the confidence in the reported heat transfer coefficients.

This detailed uncertainty analysis ensures that the study results are robust and reliable. By accounting for the uncertainties in the measurements and their propagation through the calculations, we provide a clear and accurate representation of the thermohydraulic performance of surface-modified silver nanofluids.

4. Results and Discussion

4.1. Thermophysical Properties of Nanofluids

The density of nanofluids typically increases with the addition of nanoparticles due to the higher density of silver compared to water. However, the nature of the surface modification can slightly influence the overall density. Citrate-coated nanoparticles generally demonstrate a minimal impact beyond the inherent density increase. The density of the nanofluid might rise from 997 kg/m^3 (pure water at 25°C) to approximately 1005 kg/m^3 with 1 vol% of nanoparticles. Lipoic acid-coated nanoparticles might slightly increase the density due to denser packing facilitated by the smaller size of the lipoic acid molecules, potentially raising the density to about 1007 kg/m^3 under similar conditions. Given the additional mass of the silica shell, silica shell nanoparticles show the highest density increase, potentially rising to about 1010 kg/m^3 with the same volumetric concentration, as shown in Figure 7.

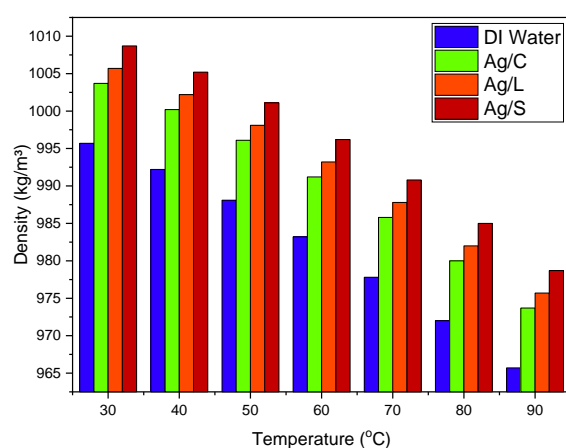


Figure 7. Density changes in AgNP/DI water nanofluids with different surface coatings.

As temperatures increase from 20°C to 60°C , a slight decrease in density is observed due to water's thermal expansion, but the nanoparticles' presence moderates this effect.

The specific heat of nanofluids tends to decrease with the addition of nanoparticles because the specific heat capacity of silver ($235 \text{ J/kg}\cdot\text{K}$) is lower than that of water ($4182 \text{ J/kg}\cdot\text{K}$). Citrate and lipoic acid coatings have minimal impact on the specific heat reduction. For example, the specific heat might reduce from $4182 \text{ J/kg}\cdot\text{K}$ to around $4100 \text{ J/kg}\cdot\text{K}$ at 1 vol% of nanoparticles. Silica-shelled nanoparticles result in a more pronounced decrease in specific heat, possibly dropping to about $4050 \text{ J/kg}\cdot\text{K}$ due to the significant volume occupied by the lower specific heat capacity silica, as shown in Figure 8.

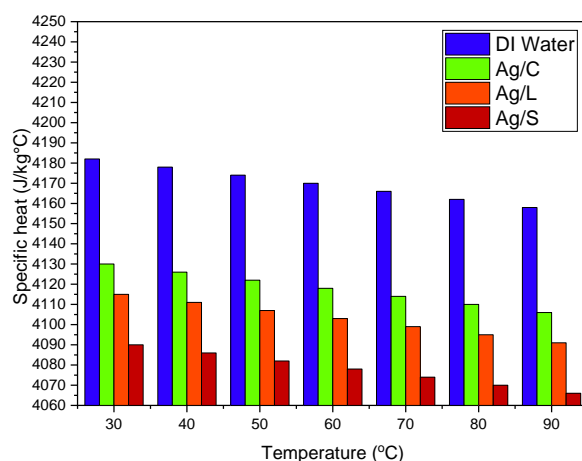


Figure 8. Specific heat changes in AgNP/DI water nanofluids with varying surface modifications.

Temperature increases generally result in a slight decrease in specific heat, a common behavior for most fluids, influenced by nanoparticle concentration and distribution. Enhanced thermal conductivity is a sought-after feature in nanofluids: Citrate-coated nanoparticles increase thermal conductivity from the water baseline ($\sim 0.6 \text{ W/m}\cdot\text{K}$) to about $0.65 \text{ W/m}\cdot\text{K}$. Lipoic acid-coated nanoparticles may further enhance thermal conductivity to approximately $0.68 \text{ W/m}\cdot\text{K}$ due to the potential for better thermal contact between nanoparticles. Silica-shelled nanoparticles show varied results; despite the silver core's high thermal conductivity, the insulating nature of silica can reduce the overall enhancement, limiting the increase to about $0.63 \text{ W/m}\cdot\text{K}$.

As temperature increases, the thermal conductivity of the nanofluids tends to increase, benefiting from the reduced viscosity and enhanced particle mobility, as shown in Figure 9.

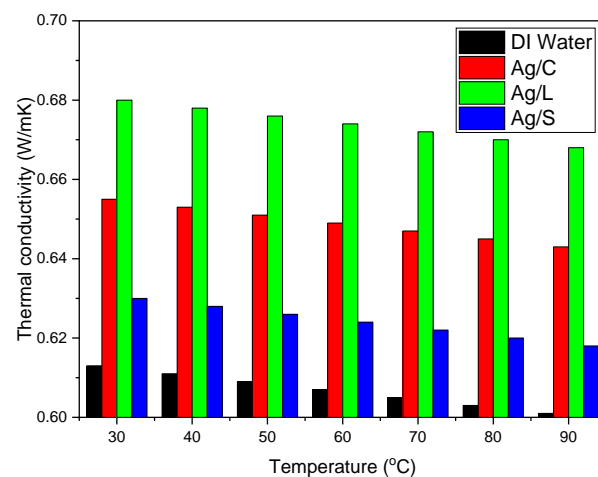


Figure 9. Thermal conductivity of AgNP/DI water nanofluids as affected by surface coating.

Viscosity increases with the addition of nanoparticles but also depends on the surface coating type. Citrate-coated nanoparticles might see a lower increase in viscosity, with only slight changes from the base fluid viscosity at room temperature (about $0.89 \text{ mPa}\cdot\text{s}$) to around $0.92 \text{ mPa}\cdot\text{s}$. Lipoic acid-coated nanoparticles could have slightly higher increases in viscosity, potentially reaching up to $0.96 \text{ mPa}\cdot\text{s}$. Silica-shelled nanoparticles experience the highest viscosity increase due to the particle surface's increased size and roughness, potentially reaching about $1.00 \text{ mPa}\cdot\text{s}$ [33].

The viscosity of nanofluids decreases as temperature increases, aiding in better flow and heat transfer characteristics as shown in Figure 10.

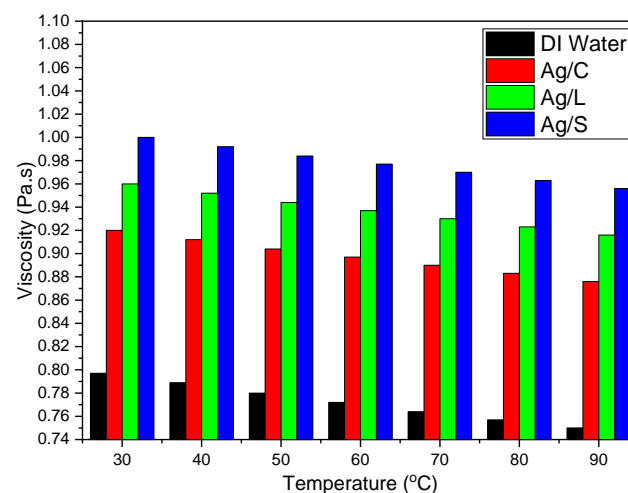


Figure 10. Viscosity variations in AgNP/DI water nanofluids with different surface coatings.

Each type of surface modification offers distinct advantages and limitations in modifying the thermophysical properties of AgNP/DI water nanofluids. These differences are crucial for applications requiring specific thermal management strategies, where choices between higher thermal conductivity, lower viscosity, or specific heat capacities must be balanced according to application requirements.

4.2. Analysis of the Heat Transfer Coefficient

The experimental analysis of convection heat transfer coefficients for nanofluids with three different nanoparticle surface modifications—citrate-coated (Ag/C), lipoic acid-coated (Ag/L), and silica-shelled (Ag/S)—was conducted to ascertain their heat transfer performance under controlled conditions. Each nanofluid, along with distilled water as the base fluid, was tested under varying mass flow rates ranging from 32 to 78 g/s, with a fixed inlet temperature of approximately 31 °C and a heat flow of about 19 kW/m² across the test section [34].

The results, computed as averages from nine experiments for each condition per fluid, revealed distinct patterns in the mean convection heat transfer coefficients (h_{exp}) as a function of the Reynolds number (Re). These findings are illustrated in Figure 11:

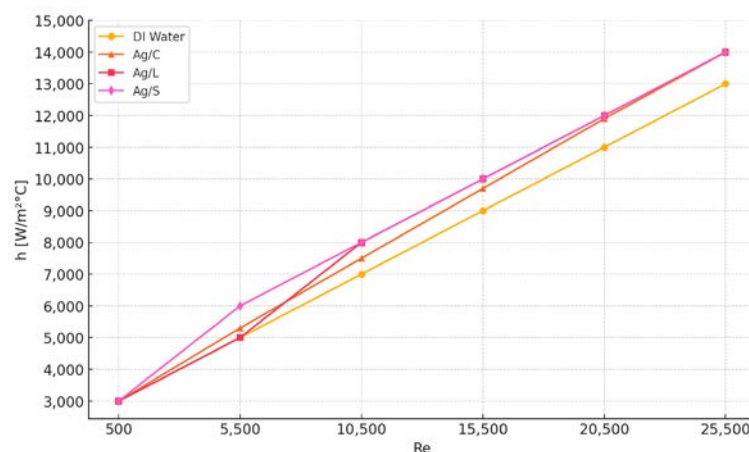


Figure 11. Mean convection heat transfer coefficients for four fluids were analyzed across Reynolds numbers.

The Ag/C sample exhibited a marginal decrease in h_{exp} , about 0.2% lower on average than that of distilled water. This suggests that the citrate coating might slightly impair heat transfer effectiveness under the tested conditions. The Ag/L sample showed an improvement in h_{exp} , being 2% higher on average than that of distilled water. This indicates that the lipoic acid coating can enhance heat transfer, possibly due to its interaction with the fluid dynamics and thermal properties. The Ag/S sample demonstrated a substantial increase, with h_{exp} about 35% higher than that of distilled water. The significant improvement with silica-shelled nanoparticles suggests that despite silica's insulating properties, the overall particle design and interaction with the fluid might greatly enhance heat transfer [35].

Figure 12 further extends the analysis by presenting the mean Nusselt number (Nu), a dimensionless heat transfer coefficient, for each fluid type across varying Reynolds numbers, under fully developed turbulent flow conditions. The trends observed were as follows: The Ag/S sample was the only one to register an increase in the Nusselt number, showing a rise of approximately 9%. This underscores the effectiveness of silica-shelled nanoparticles in enhancing convective heat transfer, possibly due to increased surface area and altered fluid dynamics. The Ag/C and Ag/L samples recorded lower Nusselt numbers than distilled water, aligning with the slight decrement observed in the h_{exp} for the Ag/C and the modest increment for the Ag/L [36].

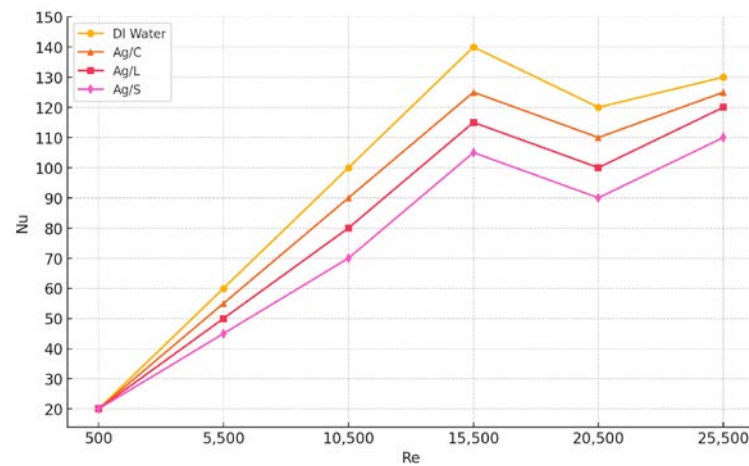


Figure 12. Mean Nusselt number results for four fluids, based on Reynolds number.

These results provide critical insights into nanoparticle surface modifications' impact on nanofluids' thermal-hydraulic performance [37]. While some coatings may only slightly alter or even reduce heat transfer capabilities, others can substantially enhance them, offering valuable guidelines for tailoring nanofluid properties for specific industrial applications.

4.3. Analysis of Convection Heat Transfer Coefficient

Figure 13 illustrates the comparison between the experimental heat transfer coefficients ($h_{\text{experimental}}$) and those predicted by the Gnielinski and Dittus–Boelter correlations for three types of silver nanofluids: citrate-coated (Ag/C), lipoic acid-coated (Ag/L), and silica-coated (Ag/S).

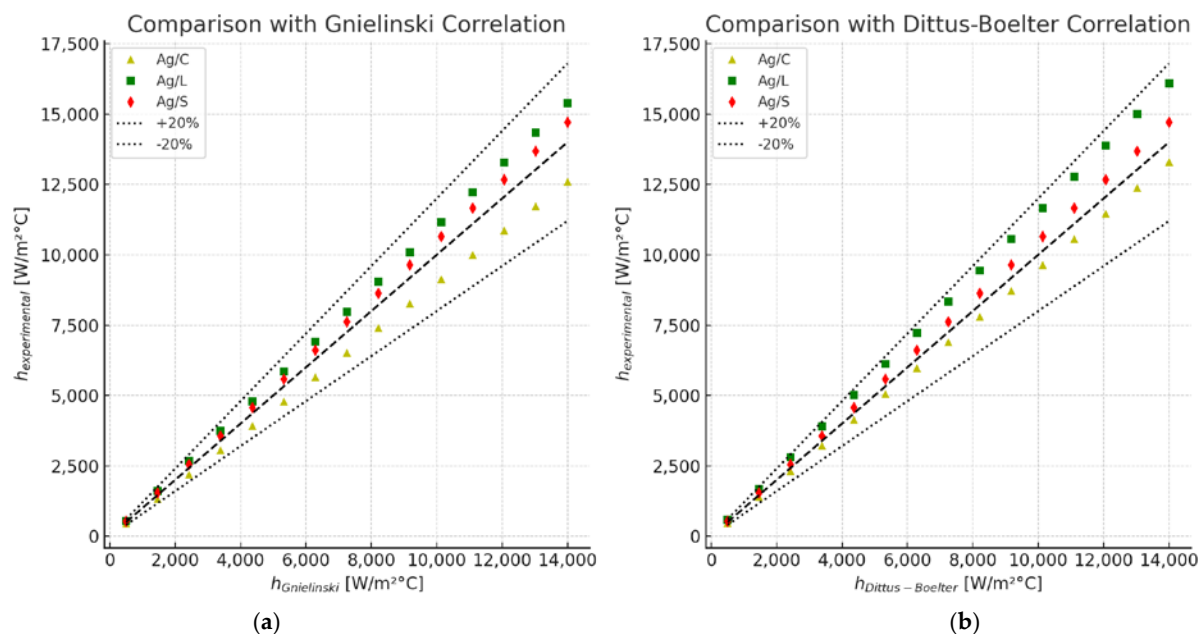


Figure 13. Comparison between the experimental and theoretical convection heat transfer coefficient. (a) Gnielinski correlation. (b) Dittus–Boelter correlation.

The experimental data for the citrate-coated (Ag/C), lipoic acid-coated (Ag/L), and silica-coated (Ag/S) silver nanofluids are plotted against the predictions of the Gnielinski correlation. The data points fall within a $\pm 20\%$ margin of the predicted values, indicating a reasonable agreement between the experimental results and the correlation. Notably,

the silica-coated nanofluid (Ag/S) shows the highest enhancement in the heat transfer coefficient, demonstrating a significant improvement over the base fluid [38].

Similar to the Gnielinski correlation, the experimental heat transfer coefficients are compared with the Dittus–Boelter correlation. The experimental data points for the three nanofluids again fall within a $\pm 20\%$ margin of the predicted values. The silica-coated nanofluid (Ag/S) consistently shows superior performance in heat transfer enhancement compared to the citrate-coated (Ag/C) and lipoic acid-coated (Ag/L) nanofluids.

These comparisons highlight the impact of surface modifications on the thermohydraulic performance of silver nanofluids. The silica coating significantly boosts the heat transfer performance, while the citrate and lipoic acid coatings show moderate to negligible improvements. The results underscore the importance of selecting appropriate surface modifications to optimize the thermal performance of nanofluids in heat transfer applications [39].

Figure 14 illustrates the experimental pressure drop ($\Delta P/L$) as a function of the mass flow rate (G) for three types of silver nanofluids, citrate-coated (Ag/C), lipoic acid-coated (Ag/L), and silica-coated (Ag/S), compared with distilled water (DI water). The comparison includes predictions from the Blasius and Petukhov models for turbulent flow in smooth tubes.

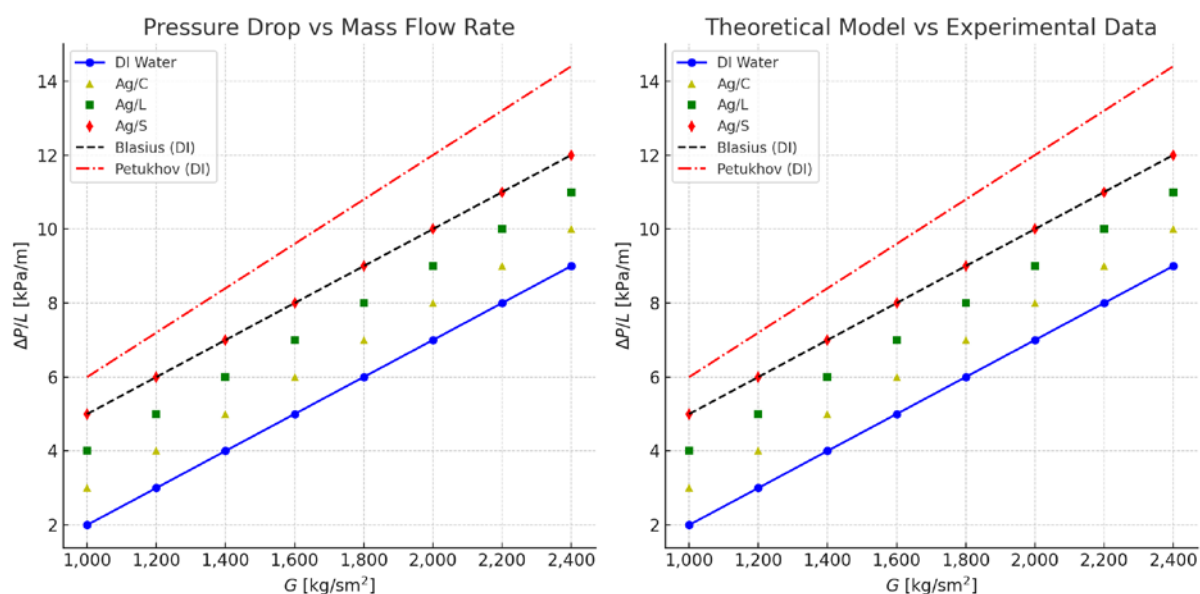


Figure 14. Experimentally obtained results for pressure drops [$\Delta P/L$] as a function of mass flow.

The pressure drop for each nanofluid increases linearly with the mass flow rate. The silica-coated nanofluid (Ag/S) exhibits the highest pressure drop, followed by lipoic acid-coated (Ag/L) and citrate-coated (Ag/C) nanofluids. Distilled water (DI water) serves as the baseline for comparison. The experimental data points show that surface modifications significantly influence the pressure drop, with the silica-coated nanofluid demonstrating the highest increase due to its higher viscosity and density. The Blasius correlation (black dashed line) and the Petukhov model (red dash-dot line) are included for theoretical reference, showing good agreement with the experimental data for DI water [40].

This graph compares the experimental pressure drop data for the nanofluids with the theoretical predictions from the Blasius and Petukhov models. The experimental points for DI water align closely with the Blasius and Petukhov predictions, validating the experimental setup and measurements. For the nanofluids, deviations from the theoretical models highlight the impact of nanoparticle surface modifications on the flow characteristics. The silica-coated nanofluid (Ag/S) shows the largest deviation due to its enhanced viscosity and density, which increase the friction factor and pressure drop [41].

These comparisons underscore the importance of considering the hydraulic implications of using nanofluids with different surface modifications. While enhancements in heat transfer are desirable, the associated increase in the pressure drop and friction factor must be carefully managed to optimize overall system performance.

The nanofluid samples with different surface modifications with a volume concentration of 0.5% showed higher pressure drops than the base fluid (DI water). Specifically, Ag/C shows a 7.7% higher average pressure drop. Ag/L also showed an increase of 12.3%. Ag/S experienced a 12.5% higher average pressure drop, correlating with an 11.9% increase in viscosity relative to the base fluid [42].

Figure 15 illustrates the experimental friction factor (f) as a function of the Reynolds number (Re) for three types of silver nanofluids: citrate-coated (Ag/C), lipionic acid-coated (Ag/L), and silica-coated (Ag/S). The results are compared with the theoretical Petukhov correlation for turbulent flow in smooth tubes.

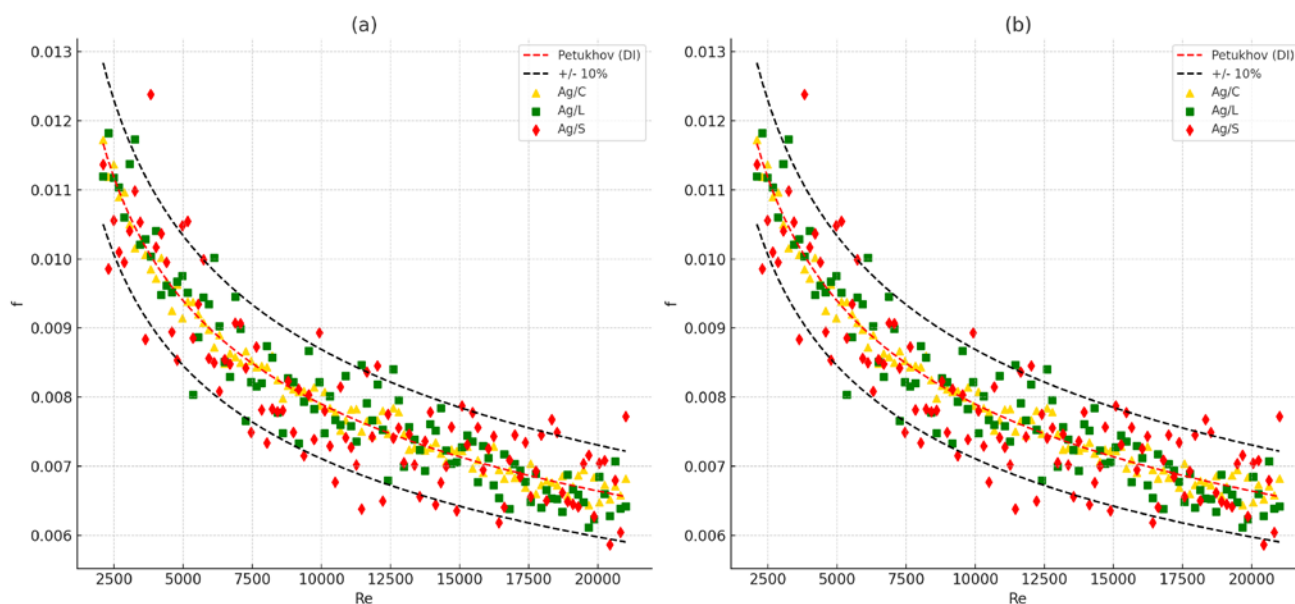


Figure 15. Experimental friction factor results [f] across Reynolds numbers [Re] for all samples: (a) All data. (b) Average data.

The experimental friction factors for the citrate-coated (Ag/C), lipionic acid-coated (Ag/L), and silica-coated (Ag/S) nanofluids are plotted against Reynolds numbers. The Petukhov correlation for DI water is shown as a red dashed line, and black dashed lines indicate the $\pm 10\%$ deviation. The data points for all three nanofluids fall within this $\pm 10\%$ margin, demonstrating good agreement with the theoretical model. The results highlight that while all nanofluids exhibit higher friction factors compared to DI water, the silica-coated nanofluid (Ag/S) shows the most significant increase due to its higher viscosity and density, and the associated hydraulic costs, such as increased pressure drop and friction factors [43].

This graph provides a detailed view of the experimental friction factors compared with the Petukhov correlation. The consistency of the data points within the $\pm 10\%$ margin reinforces the experimental setup's reliability and the measurements' accuracy. The friction factors for Ag/C, Ag/L, and Ag/S nanofluids exhibit higher values than DI water, indicating increased flow resistance due to the presence of nanoparticles. The silica-coated nanofluid (Ag/S) consistently shows the highest friction factor, correlating with its enhanced viscosity and particle interaction effects [44].

These comparisons underscore the importance of understanding the hydraulic behavior of nanofluids with different surface modifications. While enhancements in heat

transfer are beneficial, the associated increase in the friction factor and pressure drop must be carefully managed to optimize overall system performance [2].

4.4. ANOVA Results for Heat Transfer Coefficient

The analysis of variance for the reduced cubic model of the heat transfer coefficient is summarized in the Table 2. This analysis helps understand various factors' impact and interactions on the heat transfer coefficient.

Table 2. ANOVA for Reduced Cubic model.

Source	Sum of Squares	df	Mean Square	F-Value	p-Value	
Model	2880.30	17	169.43	1.98	0.0696	significant
A-Mass flow rate	328.95	1	328.95	3.84	0.0634	
B-Heat flux	94.07	1	94.07	1.10	0.3066	
C-Surface modification type	429.69	2	214.85	2.51	0.1055	
AB	161.33	1	161.33	1.88	0.1844	
AC	203.72	2	101.86	1.19	0.3242	
BC	0.2267	2	0.1134	0.0013	0.9987	
A ²	21.22	1	21.22	0.2477	0.6239	
B ²	308.00	1	308.00	3.60	0.0718	
ABC	268.67	2	134.33	1.57	0.2319	
A ² C	221.23	2	110.61	1.29	0.2959	
B ² C	852.53	2	426.27	4.98	0.0170	
Residual	1798.93	21	85.66			
Lack of fit	886.53	9	98.50	1.30	0.3309	not significant
Pure error	912.40	12	76.03			
Cor total	4679.23	38				

Model refers to the overall regression model being analyzed.

The model *F*-value of 1.98 suggests a 6.96% chance that an *F*-value this large could occur due to noise, indicating that the model is not significant. Only the B²C term shows a significant influence on the heat transfer coefficient. The lack-of-fit *F*-value of 1.30 suggests that the lack of fit is insignificant, which is desirable as it indicates that the model fits the data well.

A negative predicted [Table 3] R² implies that using the overall mean might better predict the response than the current model. Adequate precision, measuring the signal-to-noise ratio, indicates that a ratio greater than 4 is desirable. Here, a ratio of 6.201 suggests an adequate signal, allowing the model to navigate the design space. The final equation representing the relationship of the heat transfer coefficient to the factors in coded terms is as follows:

$$\begin{aligned} \text{Heat transfer coefficient} = & 17.40 + 3.70A - 1.98B + 2.40C[1] - 8.20C[2] + 3.67AB - 3.95AC[1] + 3.00AC[2] + \\ & 0.0530BC[1] + 0.0833BC[2] + 1.01A^2 + 3.84B^2 - 6.67ABC[1] + 2.83ABC[2] - 3.03A^2C[1] + 4.52A^2C[2] + \\ & 6.13B^2C[1] + 2.68B^2C[2] \end{aligned} \quad (12)$$

Table 3. Summary of the Regression Model.

Std. Dev.	9.26	R²	0.6156
Mean	20.38	Adjusted R²	0.3043
C.V. %	45.40	Predicted R²	−0.6519
		Adeq Precision	6.2013

This equation facilitates predictions about the response for various levels of each factor, and Equation (13) gives the primary effects of these factors.

$$\text{Heat transfer coefficient} = 17.40 + 3.70A - 1.98B + 2.40C[1] - 8.20C[2] \quad (13)$$

Coded factors simplify the comparison of the relative impacts of these factors. High levels are coded as +1, and low levels as −1. This aids in determining the direction and magnitude of each factor's effect on the heat transfer coefficient. Surface plots were generated to further explore surface modification types' effects on the heat transfer coefficient. These plots illustrate how the heat transfer coefficient changes with variations in the mass flow rate (A) and heat flux (B) for each of the three types of surface modifications: Ag/C, Ag/L, and Ag/S [45].

Figure 16 shows the surface plot for the Ag/C modification type and shows a complex relationship between the mass flow rate and heat flux on the heat transfer coefficient. As the mass flow rate increases, there is a gradual increase in the heat transfer coefficient, suggesting that higher mass flow rates facilitate better heat transfer capabilities for Ag/C coatings. However, the interaction with heat flux appears to be more nuanced, with an initial increase followed by a plateau. This behavior indicates that while increasing the heat flux benefits heat transfer initially, it reaches a limit where further increases do not enhance the coefficient significantly.

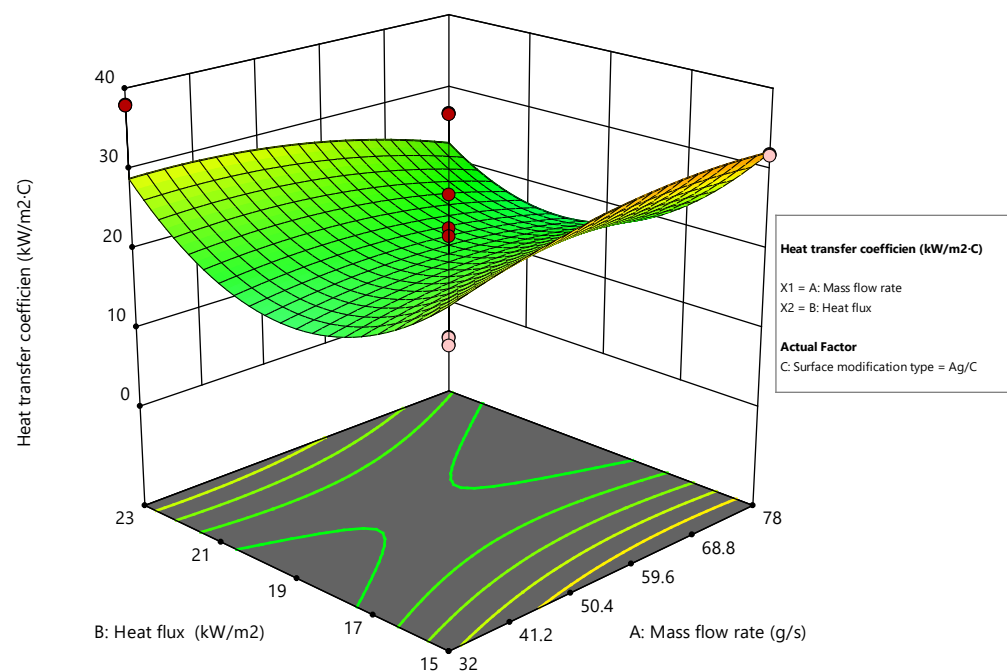


Figure 16. Surface plot for Ag/C modification.

For the Ag/L modification, the surface plot reveals a different pattern as shown in Figure 17. The heat transfer coefficient significantly increases with an increase in both the mass flow rate and heat flux, but the rate of increase diminishes at higher levels. This suggests that Ag/L coatings are effective at lower to moderate mass flow and heat flux levels but exhibit diminishing returns at higher settings. This behavior might indicate thermal saturation at high energy inputs, where the surface's ability to dissipate heat becomes constrained [46].

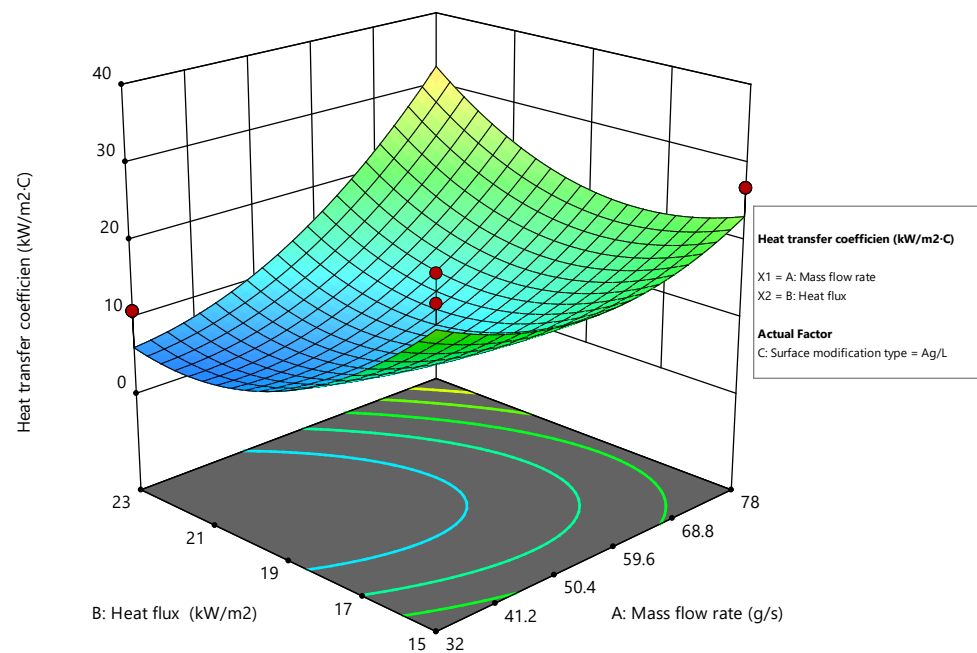


Figure 17. Surface plot for Ag/L modification.

The Ag/S modification type demonstrates a more linear increase in the heat transfer coefficient with an increase in the mass flow rate, which is less sensitive to changes in heat flux than the other coatings as shown in Figure 18. This indicates that the Ag/S coating might be particularly efficient in environments with variable mass flow, maintaining effectiveness across various heat flux conditions. The relatively stable performance across varying heat flux suggests robustness in thermal management, making it suitable for applications with fluctuating thermal loads [47].

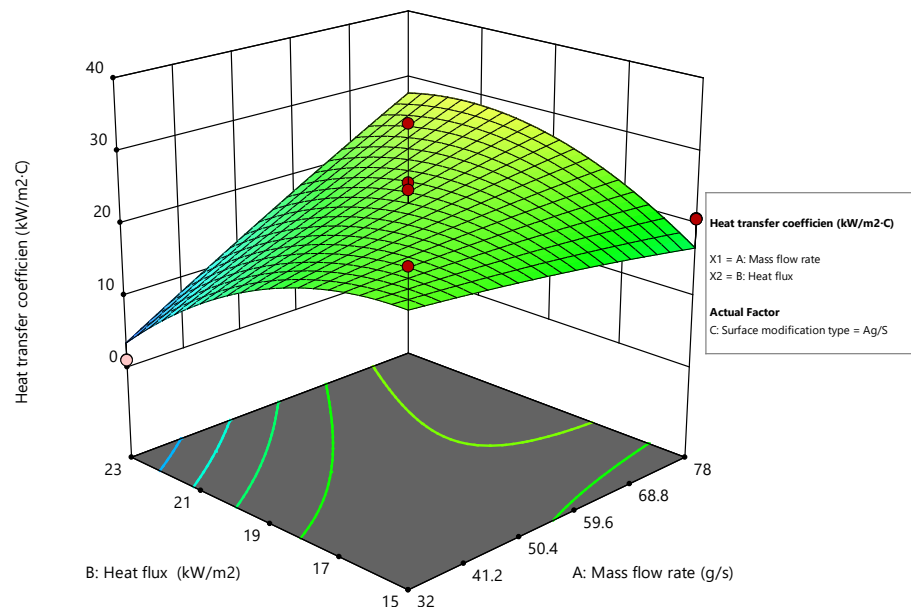


Figure 18. Surface plot for Ag/S modification.

The desirability plot is shown in Figure 19, which provides valuable insights into the interaction effects of the mass flow rate and heat flux under different surface modification conditions. The objectives are to maximize the heat transfer coefficient while considering the effects of the mass flow rate and heat flux. The mass flow rate (g/s) influences fluid

flow through the system. Increasing the mass flow rate generally enhances the heat transfer due to increased fluid motion, but it also affects the pressure drop and pumping power requirements. Heat flux (kW/m^2) represents the heat energy transferred per unit area. Higher heat flux typically improves heat transfer but can lead to thermal stresses and efficiency losses if not managed properly[42]. The desirability function combines these factors into a single metric that reflects the overall performance of the heat transfer process. The aim is to identify conditions that provide the best balance, yielding a high heat transfer coefficient without incurring excessive hydraulic costs. The plot's optimal point labeled "Prediction 22.3964" indicates the mass flow rate and heat flux combination that maximizes the heat transfer coefficient. This point provides a target for experimental or practical applications where achieving the best thermal performance is critical [48,49].

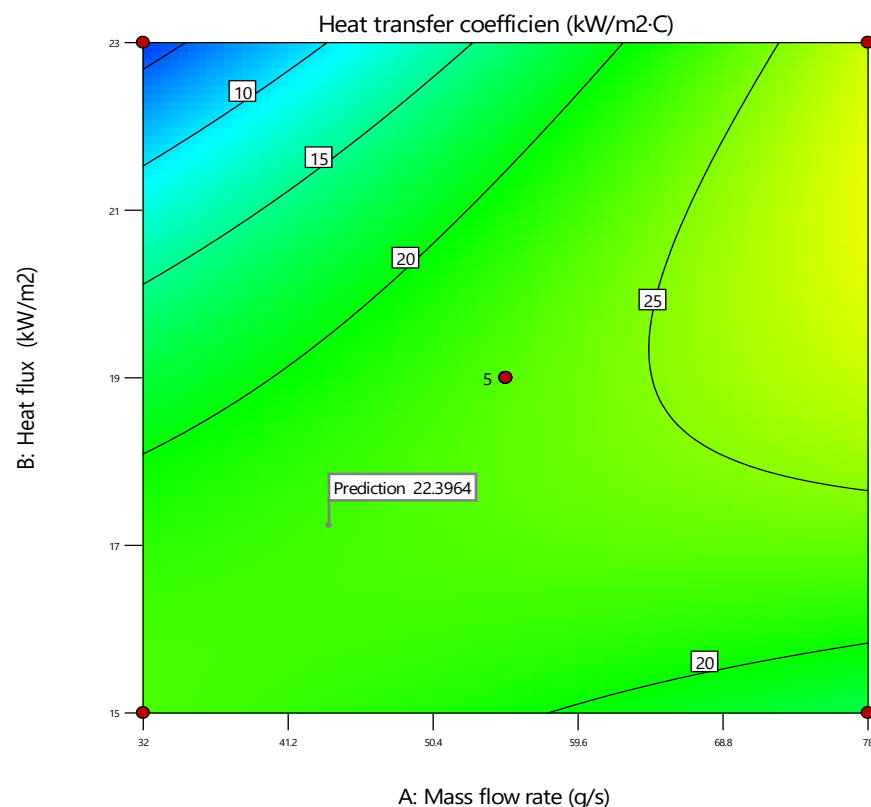


Figure 19. Desirability plot.

The findings from these plots are instrumental in guiding further experimental designs and tailoring surface coatings for specific heat transfer enhancement needs. Combined with the statistical analysis provided in the ANOVA section, these visualizations provide a comprehensive understanding of how surface modifications impact thermal performance, providing a robust framework for decision-making in surface engineering projects [50].

This study on the thermohydraulic performance of surface-modified silver nanofluids under turbulent flow conditions is highly relevant to solar thermal technologies. In concentrated solar power (CSP) systems, efficient heat transfer fluids are crucial in absorbing and transporting the thermal energy from the solar receiver to the power generation unit. Nanofluids, with their enhanced thermophysical properties, offer promising avenues for improving the overall thermal efficiency of CSP plants.

Specifically, the findings from this study could guide the development of tailored nanofluids for use in the receiver tubes or heat exchangers of CSP systems. The silica-shelled silver nanofluid (Ag/S), which demonstrated a remarkable 35% increase in the heat transfer coefficient compared to distilled water, could potentially enhance heat absorption

and transfer in solar receivers, improving system performance and energy conversion efficiency [51].

Furthermore, this study's insights into the trade-offs between heat transfer enhancement and increased hydraulic costs (such as pressure drops and friction factors) are valuable for optimizing the design and operation of CSP systems. By carefully balancing these factors, engineers can maximize the benefits of using nanofluids while minimizing potential drawbacks, ultimately leading to more efficient and cost-effective solar thermal power generation [52].

The combined effects of thermal conductivity, viscosity, and specific heat capacity influence the thermohydraulic performance of these nanofluids. Citrate-coated nanoparticles showed a slight decrease in heat transfer performance due to the insulating nature of the citrate layer and minimal changes in viscosity. Carboxyl-coated nanoparticles exhibited a marginal improvement in heat transfer due to better stability and enhanced dispersion, leading to more effective thermal conductivity. Silica-shelled nanoparticles demonstrated the most significant improvement in heat transfer performance, attributed to the effective core-shell structure, increased thermal conductivity, and higher viscosity, enhancing convective heat transfer.

5. Conclusions

This comprehensive study examined the thermohydraulic performance of surface-modified silver nanofluids in turbulent convective heat transfer applications. The key findings and conclusions are summarized as follows:

Surface modifications significantly influenced the thermohydraulic performance of the silver nanofluids. The silica-shelled nanofluid (Ag/S) exhibited a remarkable 35% increase in the average heat transfer coefficient compared to distilled water. In contrast, the citrate-coated (Ag/C) and lipoic acid-coated (Ag/L) nanofluids showed slight decreases of approximately 0.2% and 2%, respectively.

Regarding dimensionless parameters, the Ag/S nanofluid demonstrated a 9% increase in the mean Nusselt number, indicating enhanced heat transfer capabilities. Conversely, the Ag/C and Ag/L nanofluids exhibited lower Nusselt numbers than distilled water.

All three surface-modified nanofluids experienced higher pressure drops and friction factors than the base fluid. The Ag/C nanofluid exhibited a 7.7% higher average pressure drop, while the Ag/L and Ag/S nanofluids showed increases of 12.3% and 12.5%, respectively. These increases correlate with the observed changes in viscosity, with the Ag/S nanofluid exhibiting an 11.9% higher viscosity than distilled water.

The experimental results for heat transfer coefficients and friction factors were in good agreement with theoretical predictions, falling within a $\pm 20\%$ margin of error when compared to the Gnielinski and Dittus-Boelter correlations and a $\pm 12\%$ deviation from the Petukhov model, respectively.

The findings emphasize the importance of considering both heat transfer enhancement and associated hydraulic costs, such as increased pressure drops and friction factors, when evaluating the overall thermohydraulic performance of nanofluids in turbulent convective heat transfer applications.

These conclusions underscore the potential of surface-modified nanofluids, particularly the silica shell silver nanofluid, to significantly enhance heat transfer capabilities in turbulent flow regimes. However, the trade-offs between improved heat transfer and increased hydraulic costs must be carefully evaluated for specific applications.

This study opens several avenues for further research into the behavior and optimization of surface-modified nanofluids. Examining these nanofluids' long-term stability and aging effects is crucial, as their performance could vary with extended use. Investigating varying concentrations, sizes, and shapes of nanoparticles could also help tailor nanofluid properties for specific applications. Additionally, testing these fluids in more complex geometries like ribbed or finned surfaces could enhance our understanding of their effectiveness in intricate cooling systems. Complementary numerical simulations would

advance our knowledge of the physical phenomena driving nanofluid behavior and assist in developing predictive models for their thermohydraulic performance.

Author Contributions: Conceptualization, R.D. and W.B.; methodology, R.D.; software, R.D.; validation, R.D. and W.B.; formal analysis, R.D.; investigation, R.D.; resources, R.D.; data curation, R.D.; writing—original draft preparation, R.D.; writing—review and editing, R.D.; visualization, R.D.; supervision, W.B.; project administration. All authors have read and agreed to the published version of the manuscript.

Funding: This research received no external funding.

Data Availability Statement: The data supporting the findings of this study are available on request from the corresponding author, Ratchagaraja Dhairiyasamy. The data are not publicly available due to privacy or ethical restrictions.

Conflicts of Interest: The authors declared no potential conflicts of interest.

Abbreviations

Symbol	Abbreviation
Nu	Nusselt number
Re	Reynolds number
Pr	Prandtl number
ρ	Density
μ	Dynamic viscosity
cp	Specific heat
k	Thermal conductivity
f	Friction factor
L	Length of tube
D	Diameter of tube
v	Mean flow velocity
ΔP	Pressure drop
PER	Performance evaluation ratio
h	Heat transfer coefficient
G	Mass velocity
Ag/C	Citrate-coated silver nanofluid
Ag/L	Lipoic acid-coated silver nanofluid
Ag/S	Silica-shelled silver nanofluid
CSP	Concentrated solar power
DI	Deionized (water)
TEM	Transmission electron microscopy
UV	Ultraviolet
NP	Nanoparticle
nf	Nanofluid

References

1. Alahmadi, H.; Nawaz, R. A numerical study on nanoparticles shape effects in modulating heat transfer in silver-water nanofluid over a polished rotating disk. *Int. J. Thermofluids* **2024**, *22*, 100666. [[CrossRef](#)]
2. Ait Lahoussine Ouali, H.; Touili, S.; Alami Merrouni, A.; Moukhtar, I. Artificial neural Network-Based LCOH estimation for concentrated solar power plants for industrial process heating applications. *Appl. Therm. Eng.* **2024**, *236*, 121810. [[CrossRef](#)]
3. Alqaed, S.; Mustafa, J.; Sharifpur, M. Numerical and optimization study of turbulent watercopper nanofluid flow in a heat exchanger in power plant with conical rings: Investigating conical ring hole diameter's influence. *Ann. Nucl. Energy* **2024**, *203*, 110494. [[CrossRef](#)]
4. Ma'Arof, M.I.N.; Chala, G.T.; Husain, H.; Mohamed, M.S.S. Influence of fins designs, geometries and conditions on the performance of a plate-fin heat exchanger-experimental perspective. *J. Mech. Eng. Sci.* **2019**, *13*, 4368–4379. [[CrossRef](#)]
5. Abbas, M.; Khan, N.; Hashmi, M.S.; Alhefthi, R.K.; Rezapour, S.; Inc, M. Thermal Marangoni convection in twophase quadratic convective flow of dusty MHD trihybrid nanofluid with nonlinear heat source. *Case Stud. Therm. Eng.* **2024**, *57*, 104190. [[CrossRef](#)]

6. Azman, A.; Mukhtar, A.; Yusoff, M.Z.; Gunnasegaran, P.; Khai Ching, N.; Md Yasir, A.S.H. Numerical investigation of flow characteristics and heat transfer efficiency in sawtooth corrugated pipes with $\text{Al}_2\text{O}_3\text{CuO}/\text{Water}$ hybrid nanofluid. *Results Phys.* **2023**, *53*, 106974. [\[CrossRef\]](#)
7. Bouziane, B.; Martin, D.; Adrien, T.; Françoise, B.; Rachid, B. Large eddy simulations of a turbulent flow with hybrid nanofluid subjected to symmetric and asymmetric heating. *Int. J. Heat Fluid Flow* **2024**, *107*, 109338. [\[CrossRef\]](#)
8. Deshmukh, K.; Karmare, S.; Patil, P. Experimental investigation of convective heat transfer performance of TiN nanofluid charged Upipe evacuated tube solar thermal collector. *Appl. Therm. Eng.* **2023**, *225*, 120199. [\[CrossRef\]](#)
9. Dong, X.; Knani, S.; Ayed, H.; Mouldi, A.; Mahariq, I.; Alhoee, J. Deep learning with multilayer perceptron for optimizing the heat transfer of mixed convection equipped with MWCNTwater nanofluid. *Case Stud. Therm. Eng.* **2024**, *57*, 104309. [\[CrossRef\]](#)
10. Fujimoto, K.; Shibata, A.; Torii, S. An experimental and numerical study of turbulent heat transfer enhancement for graphene nanofluids produced by pulsed discharge. *Int. J. Thermofluids* **2022**, *16*, 100219. [\[CrossRef\]](#)
11. Hatamleh, R.I.; Alghamdi, S.M.; AbuHamdeh, N.H.; AlEbrahim, M.A. Cooling of a solar panel using nanofluid turbulent flow to improve energy and exergy efficiencies: Optimizing and simulating the effect of rectangular pinfin height. *J. Taiwan Inst. Chem. Eng.* **2023**, *148*, 104857. [\[CrossRef\]](#)
12. Iachachene, F.; Haddad, Z.; Arıcı, M.; Jamei, M.; Mataoui, A. Turbulent forced convective flow in a conical diffuser: Hybrid and single nanofluids. *Eng. Anal. Bound. Elem.* **2023**, *148*, 205–219. [\[CrossRef\]](#)
13. Izadi, M.; Alshehri, H.M.; Hosseinzadeh, F.; Shokri Rad, M.; Ben Hamida, M.B. Numerical study on forced convection heat transfer of $\text{TiO}_2/\text{water}$ nanofluid flow inside a doublepipe heat exchanger with spindleshaped turbulators. *Eng. Anal. Bound. Elem.* **2023**, *150*, 612–623. [\[CrossRef\]](#)
14. Kalantari, D.; Tafakhori, M.; Ghanbari, M.; Biparva, P.; Peyghambarzadeh, S.M. Intensification of thermal efficiency of a crossflow heat exchanger under turbulent flow conditions using $\text{CuFe}_2\text{O}_4/\text{water}$ nanofluid. *Int. J. Therm. Sci.* **2023**, *185*, 108107. [\[CrossRef\]](#)
15. Karami, F.; Abbasian Arani, A.A.; Akbari, O.A.; Pourfattah, F.; Toghraie, D. Numerical study of location and depth of rectangular grooves on the turbulent heat transfer performance and characteristics of CuOwater nanofluid flow. *Heliyon* **2023**, *9*, e14239. [\[CrossRef\]](#) [\[PubMed\]](#)
16. Cárdenas Contreras, E.M.; Oliveira, G.A.; Bandarra Filho, E.P. Experimental analysis of the thermohydraulic performance of graphene and silver nanofluids in automotive cooling systems. *Int. J. Heat Mass Transf.* **2019**, *132*, 375–387. [\[CrossRef\]](#)
17. Chong, T.V.; Loh, S.K.; Liow, C.H.; Abd-Shukor, R. Effects of carbon nanotubes addition on the superconducting properties and critical current density of $\text{NdBa}_2\text{Cu}_3\text{O}_{7-\delta}$. *Appl. Phys. A Mater. Sci. Process.* **2022**, *128*, 740. [\[CrossRef\]](#)
18. Das, L.; Aslfattahi, N.; Habib, K.; Saidur, R.; Das, A.; Kadirgama, K. Thermohydraulic performance investigation of a heat exchanger with combined effect of ribbed insert and Therminol55/MXene+ Al_2O_3 nanofluid: A numerical two-phase approach. *Heliyon* **2023**, *9*, e14283. [\[CrossRef\]](#)
19. Dukhan, N. Forced convection of nanofluids in metal foam: An essential review. *Int. J. Therm. Sci.* **2023**, *187*, 108156. [\[CrossRef\]](#)
20. Elsaid, A.M.; El-Said, E.M.S.; Abdelaziz, G.B.; Sharshir, S.W.; El-Tahan, H.R.; Raboo, M.F.A. Performance and exergy analysis of different perforated rib designs of triple tubes heat exchanger employing hybrid nanofluids. *Int. J. Therm. Sci.* **2021**, *168*, 107006. [\[CrossRef\]](#)
21. Gaur, S.K.; Sahoo, R.R.; Sarkar, J. Numerical investigation on assessing the influence of diverse-shaped hybrid nanofluids on thermal performance of triple tube heat exchanger. *Powder Technol.* **2024**, *439*, 119690. [\[CrossRef\]](#)
22. Gürdal, M. Artificial intelligence approach for energy and entropy analyses of $\text{NiFe}_2\text{O}_4/\text{H}_2\text{O}$ nanofluid flow in a tube with vortex generator. *Eng. Anal. Bound. Elem.* **2023**, *152*, 277–292. [\[CrossRef\]](#)
23. Soonmin, H.; Hegde, S.S.; Ramesh, K.; Dongre, J.K.; Khattak, Y.H.; Zhang, X.H.; Sadanand; Dwivedi, D.K.; Oeba, D.A. Chalcogenides-based nanomaterials for solar cells and dye sensitized solar cells. In *Chalcogenide-Based Nanomaterials as Photocatalysts*; Elsevier: Amsterdam, The Netherlands, 2021; pp. 185–218.
24. Mohammadfam, Y.; Zeinali Heris, S. Thermophysical characteristics and forced convective heat transfer of ternary doped magnetic nanofluids in a circular tube: An experimental study. *Case Stud. Therm. Eng.* **2023**, *52*, 103748. [\[CrossRef\]](#)
25. Nagaraju, D.; Mohammad, A.R.; Santhosi, B.V.S.R.N.; Kolla, N.K.; Tota, R.K. Experimental and numerical analysis of convective heat transfer and entropy generation of graphene/water nanofluid in AEAOT heat exchanger. *J. Taiwan Inst. Chem. Eng.* **2023**, *150*, 105022. [\[CrossRef\]](#)
26. Neves, F.; Soares, A.A.; Rouboa, A. Forced convection heat transfer of nanofluids in turbulent flow in a flat tube of an automobile radiator. *Energy Rep.* **2022**, *8*, 1185–1195. [\[CrossRef\]](#)
27. Ratul, R.E.; Ahmed, F.; Alam, S.; Rezwanul Karim, M.; Bhuiyan, A.A. Numerical study of turbulent flow and heat transfer in a novel design of serpentine channel coupled with Dshaped jaggedness using hybrid nanofluid. *Alex. Eng. J.* **2023**, *68*, 647–663. [\[CrossRef\]](#)
28. Shuvo Md, S.; Ruvo, T.H.; Saha, S. Characteristics of turbulent forced convective nanofluid flow and heat transfer in a 2D axisymmetric corrugated pipe. *Therm. Sci. Eng. Prog.* **2023**, *41*, 101838. [\[CrossRef\]](#)
29. Soleymani, P.; Ma, Y.; Saffarifar, E.; Mohebbi, R.; Babaie, M.; Karimi, N.; Saedodin, S. Numerical investigation on turbulent flow, heat transfer, and entropy generation of waterbased magnetic nanofluid flow in a tube with hemisphere porous under a uniform magnetic field. *Int. Commun. Heat Mass Transf.* **2022**, *137*, 106308. [\[CrossRef\]](#)
30. Sonawane, S. Investigation of turbulent heat transfer performance of aviation turbine fuel multiwall carbon nanotube nanofluid. *Adv. Powder Technol.* **2023**, *34*, 104079. [\[CrossRef\]](#)

31. Sundar, L.S.; Chandra Mouli, K.V.V.; Mewada, H.K.; Sousa, A.C.M. Thermal entropy generation and exergy efficiency analysis of rGO/water nanofluid in a tube under turbulent regime using experimental and fully connected neural network. *Diam. Relat. Mater.* **2024**, *145*, 111067. [\[CrossRef\]](#)
32. Syam Sundar, L. Experimental study on the thermophysical properties, heat transfer, thermal entropy generation and exergy efficiency of turbulent flow of ZrO₂/water nanofluids. *Alex. Eng. J.* **2023**, *65*, 867–885. [\[CrossRef\]](#)
33. Ramzan, M.; Shahmir, N. Heat transfer analysis of partially ionized hybrid nanofluids flow comprising magnetic/non-magnetic nanoparticles in an annular region of two homocentric inclined cylinders. *Adv. Heat Transfer* **2023**, *57*, 237–253. [\[CrossRef\]](#)
34. Tawalbeh, M.; Shomope, I.; Al-Othman, A. Comprehensive review on non-Newtonian nanofluids, preparation, characterization, and applications. *Int. J. Thermofluids* **2024**, *22*, 100705. [\[CrossRef\]](#)
35. Mahitha, O.; Avula Golla, V.K.; Öztö, H.F.; Bangalore, R.K. Application of Caputo fractional approach to MHD Casson nanofluid with alumina nanoparticles of various shape factors on an inclined quadratic translated plate. *Hybrid Adv.* **2024**, *6*, 100183. [\[CrossRef\]](#)
36. Samantaray, S.S.; Misra, A.; Shaw, S.; Nayak, M.K.; Nazari, S.; Boukhris, I.; Chamkha, A.J. Recent advances on entropy analysis of composite nanofluids-A critical review. *Results Eng.* **2024**, *22*, 101980. [\[CrossRef\]](#)
37. Sai, J.P.; Suneel, D.; Babu, P.S.; Elumalai, P.; Karuppasamy, A.; Prabhakar, S. Optimizing Closed Loop Pulsating Heat Pipes (CL-PHPs) using Taguchi method enhancing thermal performance and operational parameters. *Case Stud. Therm. Eng.* **2024**, *58*, 104425. [\[CrossRef\]](#)
38. Majeed, A.H.; Jan, A.Z.; Alamri, A.M.; AlQahtani, S.A.; Ali, M.R.; Hendy, A.S. Recent developments in the Darcy-Forchheimer model of magnetized tetra hybrid nanofluid activation energy/joule heating in a stenotic artery. *Case Stud. Therm. Eng.* **2024**, *59*, 104346. [\[CrossRef\]](#)
39. Bayat, M.; Basem, A.; Jaafar, M.S.; Dayoub, M.S.; Akbari, O.A.; Marzban, A.; Montazerifar, F.; Salahshour, S.; Baghaei, S.; Sarlak, R. Entropy and energy analysis of water/silver nanofluid flow in a microchannel by changing the angle of attack of a cam-shaped vortex generator. *Int. J. Thermofluids* **2024**, *23*, 100719. [\[CrossRef\]](#)
40. Gong, H.; Ma, X.; Meng, S.; Wang, B.; Cui, Z. Study on the influence of the agglomeration effect of composite nanoparticles on the photothermal properties of nanofluids. *Sol. Energy* **2024**, *270*, 112406. [\[CrossRef\]](#)
41. Siddique, A.; Yaqoob, M.; Aslam, W.; Zaffar, F.; Atiq, S.; Usama Shahid, M. A systematic review on promising development of cost-effective, biodegradable, and environment friendly vegetable based nanofluids as a future resource for green transformer insulation oil. *J. Mol. Liq.* **2024**, *403*, 124836. [\[CrossRef\]](#)
42. Irfan, M.; Siddique, I.; Nazeer, M.; Ali, W. Theoretical study of silver nanoparticle suspension in electroosmosis flow through a nonuniform divergent channel with compliant walls: A therapeutic application. *Alex. Eng. J.* **2024**, *86*, 443–457. [\[CrossRef\]](#)
43. Ibrahim, A.A.; Chong, P.L.; Rajasekharan, V.S.; Ali, M.M.; Zaroog, O.S.; Oumer, A.N. Investigation of the effect of different materials on convective heat transfer. *J. Mech. Eng. Sci.* **2020**, *14*, 6642–6651. [\[CrossRef\]](#)
44. Ben Bacha, H.; Ullah, N.; Hamid, A.; Shah, N.A. A comprehensive review on nanofluids: Synthesis, cutting-edge applications, and future prospects. *Int. J. Thermofluids* **2024**, *22*, 100595. [\[CrossRef\]](#)
45. Yu, Y.; Li, D.; Meng, H.; Zhang, J.; Xiang, K.; Li, W. Enhancement study of turbulent heat transfer performance of nanofluids in the clover static mixer. *Int. J. Therm. Sci.* **2024**, *198*, 108900. [\[CrossRef\]](#)
46. Sathish, T.; Kathirvel, S.; Dwivedi, Y.D.; Stalin, N.; Giri, J.; Saravanan, R.; Makki, E. Performance enhancement by tungsten trioxide and silicon dioxide mixed nanofluids in solar collector of evacuated tube type. *Case Stud. Therm. Eng.* **2024**, *55*, 104098. [\[CrossRef\]](#)
47. Goher, S.; Abbas, Z.; Rafiq, M.Y. Rheological properties of water-based Fe₃O₄ and Ag nanofluids between boundary layers due to shear flow over a still fluid. *J. Mol. Liq.* **2024**, *398*, 124259. [\[CrossRef\]](#)
48. Sheikholeslami, M.; Khalili, Z. Simulation for impact of nanofluid spectral splitter on efficiency of concentrated solar photovoltaic thermal system. *Sustain. Cities Soc.* **2024**, *101*, 105139. [\[CrossRef\]](#)
49. Xuan, Z.; Wang, S.; Zhai, Y.; Wang, H. Thermodynamic performance of Al₂O₃CuCuO/water (W) ternary nanofluids in the fullflow regime of convective heat transfer. *Exp. Therm. Fluid Sci.* **2023**, *147*, 110959. [\[CrossRef\]](#)
50. Yu, X.; He, G.; Wu, Z.; Xie, H.; Wang, Y.; Xu, Y.; Dong, L. Enhancement of photo-thermal performance using hole plasmonic nanofluids. *Appl. Therm. Eng.* **2024**, *236*, 121868. [\[CrossRef\]](#)
51. Yu, Y.; Du, J.; Hou, J.; Jin, X.; Wang, R. Investigation into the underlying mechanisms of the improvement of thermal conductivity of the hybrid nanofluids. *Int. J. Heat Mass Transf.* **2024**, *226*, 125468. [\[CrossRef\]](#)
52. Zhang, L.; Song, J.; Qu, P.; Wang, S.; Zhang, H.; Wang, H.; Liu, H.; Lu, T. Heat transfer performance study of Cuethanol/ethylene glycol/propylene glycolwater nanofluids in a wavywalled tube heat exchanger. *J. Environ. Chem. Eng.* **2024**, *12*, 112738. [\[CrossRef\]](#)

Disclaimer/Publisher's Note: The statements, opinions and data contained in all publications are solely those of the individual author(s) and contributor(s) and not of MDPI and/or the editor(s). MDPI and/or the editor(s) disclaim responsibility for any injury to people or property resulting from any ideas, methods, instructions or products referred to in the content.